Examining interior grid nudging techniques using two-way nesting in the WRF model for regional climate modeling

Jared H. Bowden, Tanya L. Otte, Christopher G. Nolte, and Martin J. Otte

Atmospheric Modeling and Analysis Division
U.S. EPA National Exposure Research Laboratory
Research Triangle Park, North Carolina

For submission to

Journal of Climate

04 August 2011 (revision)

Abstract

This study evaluates interior nudging techniques using the Weather Research and Forecasting (WRF) model for regional climate modeling over the contiguous United States (CONUS) using a two-way nested configuration. NCEP-Department of Energy Atmospheric Model Intercomparison Project (AMIP-II) Reanalysis (R-2) data are downscaled to 36-km $\times$ 36-km by nudging only at the lateral boundaries, using grid point (i.e. analysis) nudging, and using spectral nudging. Seven annual simulations are conducted and evaluated for 1988 by comparing 2-m temperature, precipitation, 500-hPa geopotential height, and 850-hPa meridional wind to the 32-km North American Regional Reanalysis. Using interior nudging reduces the mean biases for those fields throughout the CONUS compared to the simulation without interior nudging. The predictions of 2-m temperature and fields aloft behave similarly when either analysis or spectral nudging is used. For precipitation, however, analysis nudging generates monthly precipitation totals, intensity and frequency of precipitation that are closer to observed fields than spectral nudging. The spectrum of 250-hPa zonal winds simulated by WRF is also compared to that of the R-2 and NARR. The spatial variability in WRF is reduced by using either form of interior nudging, and analysis nudging suppresses that variability more strongly than spectral nudging. Reducing the nudging strengths on the inner domain increases the variability but generates larger biases. Our results support the use of interior nudging on both domains of a two-way nest to reduce error when the inner nest is not otherwise dominated by the lateral boundary forcing. Nevertheless, additional research is required to optimize the balance between accuracy and variability in choosing a nudging strategy.

1. Introduction

Regional climate models (RCMs) are beginning to evolve from atmospheric models into more complex regional earth system models that also include increasingly sophisticated representations of the ocean, cryosphere, land surface, and atmospheric chemistry (Leung et al., 2006). The skill of regional climate change projections should increase because these earth-system components modulate the regional-scale climate forcing. In particular, interactions due to chemistry-aerosol-cloud-radiation feedbacks is an area of needed research for climate change (Kucharski et al., 2010). To address that need, the U.S. Environmental Protection Agency (EPA) is developing a capability to downscale global climate modeling results with particular interest in understanding those feedbacks on the regional scale using the coupled Weather Research and Forecasting (WRF)/Community Multiscale Air Quality (CMAQ) model (Pleim et al., 2008). However, techniques that the EPA has applied for retrospective meteorological modeling for air quality applications are not suitable for regional climate modeling. Retrospective meteorological simulations conducted by the EPA for air quality modeling are typically reinitialized every 5.5 days and employ analysis nudging, in which Newtonian relaxation is used to adjust the model predictions at individual grid points based on the differences from gridded observations to create "dynamic analyses" (Otte, 2008). Moreover, unlike the atmosphere, which within a few days usually reaches dynamic equilibrium with the driving initial and lateral boundary conditions, the soil moisture reaches equilibrium much more slowly, with a time scale of up to a few years (Lo et al., 2008; Chen and Dudhia, 2001). The need for continuous, long-term simulations coupled with a lack of observations in future periods requires that the technique used to downscale future global climate change scenarios to study regional climate change with WRF differ from the approach used with WRF for retrospective meteorological simulations.

The EPA conducted a study of future air quality using CMAQ driven by downscaled fields from the fifth-generation Pennsylvania State University/National Center for Atmospheric Research Mesoscale Model (MM5) (Nolte et al., 2008). In that study, MM5 was used as an RCM for 10-year integrations that were relaxed toward 6-hourly lateral boundary conditions within a 15-grid-point buffer zone (Leung and Gustafson, 2005). MM5 generated persistent biases in surface temperature of 1-2 K throughout the year and modeling domain and up to 4 K in summer and dry biases of 50-80% in some parts of the modeling domain during summer (Leung and Gustafson, 2005). Some studies that focused on downscaling techniques using reanalysis data (which are generated using a different dynamical model than the RCM) have shown that the large-scale circulation in an RCM may deviate from the driving fields (Miguez-Macho et al., 2004; Castro et al., 2005). However, in the Big Brother Experiment (BBE) where the same dynamical model and physics parameterizations were used for the driving fields and the RCM, the large scales were unaffected in the RCM domain (Denis et al., 2002). In practice, most regional climate modeling applications will not have the advantages presented in the idealized BBE. Furthermore, because RCMs use spatially and temporally interpolated driving data at the lateral boundaries, it is difficult to distinguish between errors related to resolution and the representation of physical processes in the RCM versus those caused by numerical limitations at the lateral boundaries (von Storch et al., 2000; Miguez-Macho et al., 2005).

Laprise et al. (2008) state that there is a need to better understand the fundamental principles of regional climate modeling. One area they propose for further investigation is the effect of interior nudging to constrain the RCM simulation toward the driving fields. While understanding the influence of interior nudging for regional climate modeling has become an active area of research, there has been comparatively limited effort to understand the effects of interior nudging using the WRF model. Lo et al. (2008) used a one-year simulation to compare lateral boundary nudging, frequent reinitialization, and analysis nudging in the WRF model, finding that both analysis nudging and frequent reinitialization are effective to constrain the large-scale circulation and improve the accuracy of the downscaled fields. Salathé et al. (2008)

applied nudging only to the outermost nest of a triple-nested, one-way-feedback configuration of MM5 to prevent large-scale drift from the driving fields and allow mesoscale details to be developed by MM5 in the finer domains. Using the Regional Atmospheric Modeling System, Miguez-Macho et al. (2004) and Castro et al. (2005) showed that interior nudging reduces the influence of domain size on the model results, and Miguez-Macho et al. (2004) found that spectral nudging reduces the influence of the domain placement and orientation on the model results. Using the Canadian RCM, de Elía et al. (2008) and Alexandru et al. (2009) found that spectral nudging decreases spurious precipitation at outflow boundaries, reduces extreme precipitation frequency and intensity, and reduces surface temperature error compared to nudging only at the boundaries. Overall, however, little is known about the impacts of large-scale interior nudging for regional climate modeling, so the choice of whether or not to use nudging is left to the researcher's judgment (de Elía et al., 2008).

This study provides additional insights into the advantages and limitations of using interior nudging for continuous integrations in the WRF model for regional climate modeling applications. Understanding the advantages and limitations of the nudging strategies within WRF is critical because WRF is increasingly being used as a regional climate model for various important applications including both seasonal forecasting and climate change projections. This paper does not comprehensively address all aspects of using nudging in WRF for regional climate modeling; rather we focus on available techniques in WRF and make changes to the default settings. One specific challenge in regional climate modeling not addressed is the issue of horizontal domain size dependence. We chose not to focus on the horizontal domain size issue because the spectral nudging technique implemented in WRF follows that of Miguez-Macho et al. (2004) which demonstrated that spectral nudging can be used to eliminate the effects of horizontal domain size dependence.

In this paper, the 2.5º × 2.5º NCEP-Department of Energy Atmospheric Model Intercomparison Project (AMIP-II) Reanalysis data (Kanamitsu et al., 2002) (hereafter, R-2) are downscaled using WRF with three nudging techniques: nudging only at the lateral boundaries using a five-grid-point buffer zone (Davies, 1976) (i.e., no interior nudging), grid point (analysis) nudging, and spectral nudging. While Lo et al. (2008) investigated a similar topic by also using a one-year period, we use two-way interactive nesting rather than a single domain, and we compare the analysis and spectral nudging techniques in WRF for downscaling. We also conduct additional simulations to better understand how the nudging techniques should be applied for two-way nesting in WRF. Using reanalysis data satisfies a prerequisite for estimating climate change projections by assessing the ability of the model to simulate current climate and its physical processes (Laprise et al., 2008). The R-2 is selected because it is comparable to the resolution of the NASA Goddard Institute for Space Studies (GISS) ModelE, which is being used in a parallel effort to understand how techniques developed here can be applied to fields from a general circulation model (GCM). The ultimate goal is to apply downscaling methodologies developed using verifiable R-2 fields and WRF to downscale the GISS ModelE fields for regional climate change assessments. Section 2 of this paper describes the WRF model configuration and the nudging strategies. In section 3, we examine annual biases near the surface and aloft for six regions of the contiguous United States (CONUS) for seven 14-month simulations. We also present frequency distributions, and we use spectral decomposition to examine the variability in WRF compared to R-2. Lastly, concluding remarks are given in section 4, with recommendations for areas of future research.

2. Model and experimental design

The WRF model (Skamarock et al., 2008) is a fully compressible, non-hydrostatic model that uses a terrain-following vertical coordinate. A two-way interactive nest is used with horizontal grid spacings of 108 km (81 x 51 grid points) and 36 km (187 x 85 grid points) (Fig. 1), and 34 vertical layers extending to 50 hPa. Although WRF has been used with increasing confidence for regional climate modeling studies (Leung and Qian, 2009; Bukovsky and Karoly, 2009), no suite of model options has been universally recommended for all regional climate studies. For this study, WRF version 3.2 is used, and the physics options are the Kain-Fritsch convective parameterization, WRF single-moment 6-class microphysics scheme, Yonsei University planetary boundary layer (PBL) scheme, Noah land-surface model, and the Rapid Radiative Transfer Model for GCMs for longwave and shortwave radiation. The simulations use time-varying sea-surface temperatures, sea ice, vegetation fraction, and albedo. We recognize that other WRF model configurations may lead to a better representation of the climate (both regionally and seasonally) than the configuration selected here. This study does not alter the model physics, domain size, or resolution because we emphasize evaluating the nudging strategy. We do not consider horizontal domain size dependencies because the spectral nudging technique implemented in WRF follows that of Miguez-Macho et al. (2004) which demonstrated that spectral nudging eliminates the effects of the horizontal domain size dependence. Because the physical processes that govern regional climate vary spatially, we created six regions for model verification (Fig. 1) that are similar to those used in Nolte et al. (2008). When interior nudging is applied in this study, only information from R-2 is used, and no additional observational data are used to enhance R-2 for initial and lateral boundary conditions or the analyses used for interior nudging. The goal is to understand the potential of interior nudging for regional climate change applications where only GCM data exist. Retrospective regional climate applications that require higher spatial resolution, particularly in regions of the world that are data rich, may employ a different nudging strategy than the methods examined here.

WRF is used to downscale R-2 for 1988 when most of the CONUS experienced drought conditions (Namias, 1991). Tens of billions of dollars and thousands of lives were lost in the 1988 drought, in which a strong La Niña shifted the large-scale circulation in mid-latitudes, displacing the jet stream and associated storm tracks northward of their climatological positions (Trenberth and Guillemot, 1996). This study focuses on 1988 because the transient eddies were located farther north and were much weaker over the CONUS than normal. How nudging affects transient wave activity has important implications for future climate downscaling applications in the mid-latitudes, with a predicted poleward shift in storm tracks (Yin, 2005), as well as for regional climate modeling in the equatorial tropics, where there are fewer transient eddies.

Three nudging techniques are investigated for regional climate modeling to determine the impacts on the mean error and variability using WRF. Seven simulations are conducted using various interior nudging strategies (Table 1). Each simulation is initialized at 00 UTC 1 November 1987, allowed to spin up for two months, run through 00 UTC 1 January 1989, and analyzed for 1988. The simulation that nudges only at the lateral boundaries contains no interior nudging ("NN"). The other simulations use grid-based four-dimensional data assimilation techniques in WRF: analysis nudging ("AN") and spectral nudging ("SN"). The analysis nudging technique is typically used when input fields are not significantly coarser than the target resolution, as in retrospective meteorological simulations used for air quality. Analysis nudging uses an artificial tendency term in the prognostic equations to relax each grid point towards the difference from a value that is interpolated in time from the analyses (Stauffer and Seaman, 1994). In the WRF model, analysis nudging is applied to the u and v wind components, potential temperature, and water vapor mixing ratio. The nudging term for each of those fields is scaled by a relaxation coefficient (i.e., nudging strength) that is inversely proportional to the *e*-folding time that would be required to adjust the model to the observed state in the absence of other (physical) forcing. In WRF, analysis nudging can be restricted to certain model layers and/or above the PBL. This feature is advantageous because RCMs should be allowed to respond to mesoscale forcing in the PBL while being constrained by large-scale features in the coarser input data. Three variations of analysis nudging are tested by altering the nudging strengths in the inner and outer domains (Table 1).

By contrast, spectral nudging is attractive when input fields are coarser than the target resolution. Spectral nudging adds new terms to the prognostic equations to relax the RCM toward selected wavelengths in the input data (Miguez-Macho et al., 2005). As implemented in WRF and similar to analysis nudging, nudging coefficients for spectral nudging are specified for u and v wind components and potential temperature. Unlike analysis nudging, there is no spectral nudging of moisture, but total geopotential can be nudged. Spectral nudging can also be restricted to above the PBL or a prognostic model level. The minimum wavelength for spectral nudging corresponds to the minimum wavelength resolved in the input fields, and the minimum wavelength resolved should be at least $4\Delta x$ (Pielke, 2002), which is ˜1100 km for R-2 in mid-latitudes. All spectral nudging simulations in this study nudge wavelengths larger than 1200 km in the 108-km and inner 36-km domains. As with analysis nudging, we use three variations on spectral nudging where the strengths are adjusted on the inner and outer domains (Table 1). There is no interior nudging in the PBL in any simulations conducted here.

3. Results and discussion

The 36-km WRF simulations are evaluated against the 32-km North American Regional Reanalysis (NARR) (Mesinger et al., 2006), which is bilinearly interpolated to the 36-km WRF domain. The NARR data have been found to compare well independently with observations over land within the CONUS (Mesinger et al., 2006). For instance, precipitation in NARR is found to be well represented over the CONUS including the ability to represent extreme events and organized convection (Bukovsky and Karoly, 2007). Evaluation using the NARR data is generally for large regional averages and entire seasons. At these spatial and time scales NARR performance for the variables used in this study is robust, especially over the CONUS.

Biases in the simulated large-scale circulation in the upper and lower troposphere are analyzed by examining the 500-hPa geopotential height and the 850-hPa meridional wind fields. Mean biases in the 2-m temperature and precipitation fields are calculated for regions of the

CONUS (Fig. 1) for daily, monthly, seasonal, and annual averaging periods. We supplement the mean biases with biases in the 5th and 95th percentile for daily mean temperature and the 95th percentile daily precipitation, providing additional insights into the seasonality of the temperature bias and intensity of the extreme precipitation events. Distributions of daily temperature and precipitation from the WRF model are compared against NARR to gauge WRF's ability to simulate the frequency of the extremes. Our seasonal definitions are atypical because we evaluate only the twelve-month period in 1988. So, for this study, winter, spring, summer, and fall are January-February-March (JFM), April-May-June (AMJ), July-August-September (JAS), and October-November-December (OND), respectively. However, we examine the low-level circulation in the summer (JJA) because the strength of the Great Plains low-level jet is greatest during this season.

a. Thermodynamic and dynamic fields

To begin, we examine fields that reflect the large-scale circulation and could be modulated by interior nudging. Without interior nudging, the 500-hPa geopotential height field is generally overestimated throughout the CONUS in NN for most seasons compared to NARR (Fig. 2). During the spring, NN underestimates the average strength of coastal low pressure troughs compared to the NARR by more than 40 m. Systematically underestimating the average intensity of these 500-hPa troughs results in weaker and less accurate depictions of these weather systems, which are important for regional climate. Interestingly, during periods of less active weather, such as zonal flow during the summer, the modeled heights in NN remain positively biased. As shown in Fig. 3, the seasonal 500-hPa geopotential height fields in AN and SN are very similar, with biases reduced to 15 m or less for large areas of the CONUS. Overall, the bias in 500-hPa geopotential height is small, though consistenly positive for all regions and seasons, which is also consistent with the warm biases in 2-m temperature (Table 2).

Looking toward the surface, the 850-hPa meridional wind field includes some mesoscale features that are not in the coarse R-2 but could be developed by WRF as an RCM. The meridional wind field (derived from the grid-relative u- and v-component winds in WRF) is directly affected by interior nudging at some locations and times, depending on the surface pressure and the height of the PBL. Figure 4 shows the 850-hPa JJA meridional wind bias relative to NARR for the NN, AN, and SN simulations. The climate in different regions of the CONUS is controlled by different physical mechanisms, e.g., the strength, placement, and timing of the low-level jet over the Plains. Without interior nudging (NN), the southerly 850-hPa meridional wind is underestimated over the Plains, which adversely affects moisture transport from the Gulf of Mexico. Both interior nudging techniques reduce this underestimation of the 850-hPa meridional jet, and AN and SN reduce the error in the 850-hPa meridional wind to less than 1 m s^{-1} for most areas of the CONUS. The meridional wind responsible for moisture flux into the Southeast is much weaker in NN than in NARR, and it is more realistic in AN and SN than in NN. However, AN and SN have greater error than NN in the Pacific (off the coasts of southern California and the Baja California peninsula of Mexico) and south Texas, where the strength of the 850-hPa meridional wind is overestimated by more than 2 m s^{-1}. Figures 3 and 4, together with the meridional wind bias in other seasons (not shown), demonstrate that AN and SN adjust the atmospheric circulation throughout the year for both the upper and lower atmosphere in very similar ways. In overcoming some of the model deficiencies that contribute to larger biases in NN, both interior nudging techniques improve the large-scale circulation simulated by WRF.

To determine the effects of nudging on a field that is not directly adjusted by interior nudging, biases in the mean and 5^{th} and 95^{th} percentile daily averaged 2-m temperature are examined over the annual cycle. When interior nudging is not used (NN), there is a systematic warm bias for the mean temperature in all six regions of the CONUS compared to the NARR (Table 2), which is consistent with the overestimation of 500-hPa geopotential height shown in Fig. 2.

The mean bias is at least 1.8 K in all regions. The largest temperature bias in NN, 4.3 K, is in the Plains region, which is in the center of the 36-km domain and the farthest from the lateral boundaries. A temperature bias of several degrees is undesirable because it may be as large as the climate change signal (Giorgi, 2006). Using interior nudging techniques in AN and SN reduces the mean bias in annual-averaged daily 2-m temperature by at least 1 K in all regions and by as much as 2.7 K. As in NN, the largest mean biases in AN and SN are in the Plains region. SN has a consistently cooler bias than AN, but the sign of the bias can be regionally different.

We use bias in the 5$^{\text{th}}$and 95$^{\text{th}}$ percentile daily temperature for the annual cycle to examine the seasonality in the bias, with the 5$^{\text{th}}$ percentile representing the colder temperatures in the winter and the 95$^{\text{th}}$ percentile representing the warmer temperatures in the summer. For the NN simulation, the bias in the 5$^{\text{th}}$percentile temperatures is greater than the bias in the mean throughout the CONUS. This larger wintertime bias is consistent with Fig. 2, which shows the representation of the large-scale circulation is worse in OND than in the other seasons, perhaps because the synoptic systems, which are poorly captured in NN, tend to be strong during the fall and winter. The reduced bias of the 5$^{\text{th}}$ and 95$^{\text{th}}$percentile daily 2-m temperature for both AN and SN demonstrates that interior grid nudging improves the representation of both extremes, cold and warm temperatures. The reduction of error in both AN and SN compared to NN shows that using interior nudging to constrain WRF above the PBL can also have a positive impact on fields that are not directly nudged.

Figure 5 shows the annual cycle of monthly mean 2-m temperature for NN, AN, and SN compared to NARR for each of the six regions. The NN configuration has a warm bias compared to NARR in four of the six regions throughout the year. Interior nudging reduces the positive bias, as both AN and SN generate regional 2-m temperatures that are more consistent with NARR than NN. In particular, interior nudging reduces the winter and summer biases in the Northwest, Southwest, Plains, and Southeast regions. In addition, interior nudging in both AN and SN reduces the summertime cold bias of NN in the Northeast region, demonstrating that interior nudging does not simply systematically cool the near-surface temperatures in WRF. Nudging toward the R-2 fields above the PBL effectively constrains the model so that simulated 2-m temperatures on the 36-km domain are more consistent with the 32-km NARR.

Both forms of interior nudging produce simulations of 2-m temperature that are closer to observations (represented by NARR) than limiting nudging to the lateral boundaries. However, neither form of interior nudging completely corrects all of the seasonal and regional errors in 2-m temperature. East of the Rockies, interior nudging reduces the mean 2-m temperature bias compared to NN more effectively in the summer than in the winter (Fig. 5, Plains region). This suggests that interior nudging cannot overcome the mismatch in describing the underlying terrain between WRF and R-2 and its influence on the resulting terrain-induced atmospheric wave structures because the atmospheric waves are stronger in winter than summer. Both AN and SN reduce the bias in the daily mean 2-m temperature in NN relative to NARR (Fig. 6), but both simulations with interior nudging have pronounced winter warm biases of 3-5 K in the Plains region. Fig. 6 compares the daily 2-m temperature bias with the daily geopotential height bias in the Plains. There is a strong correlation between the height bias and 2-m temperature bias in the NN case that is not apparent in either AN or SN. The NN simulation often captures large temperature swings associated with synoptic systems in the Plains (not shown), but the intensity of the systems, as reflected in the biases in geopotential height and temperature, is often misrepresented. Interior nudging helps to correct WRF's representation of the intensity of those weather systems and daily weather features, as AN and SN both have consistently smaller errors in daily mean 2-m temperature and geopotential height than NN.

The distribution of daily-averaged 2-m temperature over the annual cycle for all land points in the 36-km domain is shown in Fig. 7. The tails of the temperature distribution represent the colder and warmer locations in the domain rather than the temperature extremes at a given grid point. In NN, the distribution is shifted towards a warmer climatology than NARR for all 2-m temperature bins, which is consistent with the warm bias shown in Figs. 5 and 6. For both AN and SN, the frequency of daily mean 2-m temperatures >300 K, generally representing places with warmer climatology, is well simulated. The frequency of cooler temperatures (i.e., 265-280 K) is improved but remains underestimated. SN has a distribution of daily mean 2-m temperature that is slightly closer to NARR than AN is at the tails of the distribution (i.e., <265 K and >300 K). All three WRF simulations overestimate the distribution of daily mean 2-m temperatures between 280 and 300 K, which suggests that there are some areas in the WRF physics that could be targeted for improvement for regional climate modeling.

b. Precipitation

Accurate repesentation of precipitation and the water cycle is critical for regional climate modeling applications. As shown in Table 3, NN is wetter than observed in all six regions of the CONUS, and the mean precipitation bias for NN is generally larger than both of the nudged runs. Recall that 1988 was a drought year. In the absence of interior nudging, WRF in RCM mode uniformly overpredicts precipitation. SN reduces the mean precipitation biases in NN compared to NARR for five of the six regions of the CONUS. However, AN uniformly reduces the mean precipitation bias in all six regions, and it has a stronger impact to minimize the bias than SN. As shown by the positive bias in the 95$^{\text{th}}$ percentile, the heavy precipitation events in NN are much stronger than observed for most of the CONUS. Both AN and SN generally improve the representation of the extreme precipitation events, but the 95$^{\text{th}}$ percentile remains higher than observed. Some previous examinations of spectral nudging have focused on periods characterized by frequent wave activity resulting in intense convection and heavy precipitation (e.g., Midwestern United States floods in spring 1993; Miguez-Macho et al. (2004); Castro et al. (2005)), where spectral nudging improved the simulation of precipitation. However, under the drought conditions in 1988 and using WRF, we find that spectral nudging only slightly improves the mean precipitation biases, and actually worsens the bias in the Plains. Because AN has a greater impact on the annual mean precipitation bias than SN, we speculate that the spectral nudging techniques used in WRF could be better optimized for regional climate modeling.

As shown in Table 3 for precipitation, unlike 2-m temperature, the mean precipitation biases using AN and SN are very different from each other (Fig. 8). The strong seasonal cycle in the Northwest with more precipitation in the winter than in the summer is captured in all three simulations, most likely because this region is strongly influenced by the inflow imposed at the western lateral boundaries. The precipitation in the Northwest is closest to NARR in AN, as both SN and NN overestimate the regionally averaged monthly accumulated precipitation by ˜15-60 mm during the rainy months. In the Southwest, which is also influenced by the inflow boundaries, monthly accumulated precipitation is generally overestimated, with many months having a positive precipitation bias exceeding 20 mm for NN and SN. The monthly accumulations improve with AN for the Southwest region. The prediction of precipitation in the Plains, which is farther from the lateral boundaries, is similar to the Southwest, as AN improves monthly totals with respect to NN, and the monthly variability is better represented in AN. The Midwest accumulated precipitation in SN and NN have wet biases while AN is too dry. However, AN significantly improves the representation of the monthly variability over the Midwest. In the Northeast SN captures the monthly variability, but the monthly regionally averaged accumulations are biased high by 30 mm on average. AN better represents the monthly totals and captures the monthly variability in the Northeast. The Southeast is the only region where AN does not consistently outperform NN and SN for the monthly accumulated precipitation. In that region, AN overestimates monthly accumulated summer precipitation by $>$60 mm and underestimates the monthly accumulated winter precipitation by 20-30 mm. In the absence of interior nudging, NN captures the interseasonal variability only for regions with a robust annual cycle such as the Northwest. Both interior nudging techniques improve the intraseasonal and interseasonal variability of precipitation, particularly for regions that are less strongly controlled by the lateral boundaries. AN generally improves the monthly precipitation amount for most regions and seasons.

To determine the influence of individual weather events on the monthly totals in Fig. 8, the distribution of daily averaged precipitation for all land points in the 36-km domain is shown in Fig. 9. Without interior nudging, NN overestimates the frequency of light precipitation events (i.e., $<$5 mm day^{-1}) and underestimates the frequency of heavy precipitation events (i.e., $>$20 mm day^{-1}). In conjunction with the previous results, there are fewer heavy precipitation days, but the precipitation events tend to be more intense in WRF than in NARR. It is important to note that the calculation of the frequency of the precipitation events (Fig. 9) uses grid cells, while the intensity (Table 3) is determined using area averages. Qualitatively, SN behaves similarly to NN for the binned daily precipitation totals, but SN verifies closer to the analyses in NARR than NN does. Consistent with Fig. 8, AN improves the precipitation distribution relative to NN and SN, most notably by decreasing the number of lighter rainfall events and increasing the frequency of heavy rainfall events so that the distribution better matches NARR. The moisture field can be adjusted with analysis nudging but not by spectral nudging in WRF. This adjustment may improve the representation of the mean precipitation and frequency and may explain why AN agrees better with observations of total precipitation than SN does. The differing responses of the precipitation in WRF to the two interior nudging techniques also suggest that there are mechanistic differences in the model that result from altering the physical equations for nudging, so additional exploration of the influences of nudging on the model physics should be considered.

c. Spectral analysis

To examine the effects of interior nudging on regional-scale variability, the one-dimensional power spectrum of the domain-wide 250-hPa zonal winds is computed. The winds aloft were chosen because of the large-scale energy associated with the jet stream. The added variability from the RCM (which does not necessarily represent added value) is inferred using spectral analysis. The power spectra in this study are calculated using a discrete one-dimensional Fourier transform after removing a linear trend from the atmospheric field in the RCM domain (Skamarock, 2004). The spectral energy in each wavenumber at 6-hour intervals is computed for the R-2, NARR, and WRF model simulations, then averaged for the domain and over all times. Spectra from the WRF and regridded R-2 are compared to provide information about the large-scale variability generated by WRF. The small-scale variability in the WRF simulations (i.e. wavelengths smaller than R-2) are compared against NARR. As in Castro et al. (2005) and Rockel et al. (2008), the minimum resolvable wavelength of a discrete model is $4\Delta x$, which corresponds to a wave number of 5.65×10^{-6} m^{-1} for R-2 (i.e., a wavelength of ˜1100km in mid-latitudes). Using these criteria, the minimum resolved wavelength for the WRF 36-km domain is 144 km, or a wave number of 4.36×10^{-5} m^{-1}. Between those two values are the wavelengths where the RCM should be able to add variability and possibly value by downscaling the R-2.

Figure 10 shows the power spectrum of 250-hPa zonal winds averaged for January and July comparing NN, AN, and SN WRF simulations to R-2 and NARR. At wavelengths longer than $4\Delta x$ of R-2 during January, all simulations have a tendency to follow the R-2, but in July there is more divergence in the spectra at the longer wavelengths. The differences in the spectra may be partially explained by the weaker zonal winds during the summer as the jet stream retreats further north. At the smaller wavelengths, for both January and July, we find that the AN simulation variance is smaller than NN, SN and NARR. We also note that the spectrum variance in WRF when compared to NARR has some unrealistic decay with decreasing wavelengths, which is illustrated by the change in the slope of the spectra. Overall, Fig. 10 indicates that analysis nudging can consistently dampen the RCM variability compared to both NN and SN for January and July. However, this configuration of analysis nudging that was used in AN improves the mean precipitation, precipitation distribution and intensity of heavy rainfall events, which highlights one of the trade-offs of using interior nudging techniques.

d. Interior nudging with reduced coefficients

The initial WRF simulations for 1988 using interior nudging (AN and SN) improved the overall simulation in comparison with limiting nudging to the lateral boundaries (NN). However, SN was not able to improve the simulated precipitation as well as AN (Tables 2 and 3 and Figs. 8 and 9), and AN suppressed variability in the 250-hPa zonal wind spectra compared to SN and NN (Fig. 10). Four additional simulations, Table 1, are performed to examine the sensitivity of simulated mean errors and variability to the interior nudging strength. In the first two simulations (ANlow and SNlow), weaker nudging (and, thus, a weaker constraint toward the R-2) is used on both the 108-km and 36-km domains by reducing the nudging coefficients by one order of magnitude. In the final two simulations (ANouter and SNouter), the nudging coefficients remain unchanged from AN and SN in the 108-km domain, but they are reduced to zero (i.e., no nudging) on the 36-km domain.

Figure 11 shows the mean bias in the 500-hPa geopotential height during the fall season (OND) for ANlow, ANouter, SNlow, and SNouter; the results are qualitatively similar for the other seasons (not shown). When nudging is used on the 36-km (inner) domain, the bias in the large-scale circulation is reduced by ~25 m over most of the domain (compare Figs. 3 and 11 to Fig. 2). Reducing the nudging coefficients on both domains increases the height bias by <5 m for the weakly nudged simulations (ANlow and SNlow) compared to AN and SN. By contrast, eliminating the interior nudging on the 36-km domain (ANouter and SNouter) increases the mean error in 500-hPa geopotential height to >35 m in the Plains and Southwest. The magitude of the bias in 500-hPa geopotential height tends to increase farther from the lateral boundaries when either spectral or analysis nudging is applied only to the 108-km (outer) domain. Even with two-way interaction in the interior of the 36-km domain and lateral boundary forcing from the nudged 108-km domain, the error in the 500-hPa geopotential height in the 36-km domain is noticeably larger when interior nudging is not directly applied to the 36-km domain. Our results show that using interior nudging with a non-zero strength on the innermost domain of a two-way-nested configuration (here, on the 36-km domain) is necessary to constrain the large-scale circulation in the interior of the domain if it is not otherwise dominated by lateral boundary forcing.

The 850-hPa meridional wind during JJA for the sensitivity simulations is shown in Fig. 12. The ANlow and SNlow bias is similar to the AN and SN bias in Fig. 4. Figures 4 and 12 indicate an overestimation in the meridional wind for the Great Plains low-level jet over portions of Texas, overestimation of the meridional winds off the coast of California and an underestimation over the Baja California peninsula. Removing nudging on the interior domain increases errors in simulated meridional winds throughout the entire domain. The positive bias becomes larger over Texas and portions of the Pacific Ocean, and there is also an underestimation in the meridional wind for northern portions of the Plains region into the Midwest. Interestingly, there are significant differences between ANouter and SNouter in the meridional wind bias for the eastern half of the US. The SNouter simulation results in positive bias along the east coast of the US, while the bias is slightly negative to near zero in the ANouter simulation. Despite these differences, both SNouter and ANouter show there is a general degradation in the low-level circulation when nudging on the inner domain is not applied.

Table 2 shows the biases in mean and 5^{th} and 95^{th} percentile 2-m temperature for the various nudging sensitivity tests. Reducing the nudging strengths by one order of magnitude in ANlow and SNlow results in little difference (<0.5 K for most regions) when compared to AN and SN. When nudging is not used in the 36-km domain (ANouter and SNouter), the mean 2-m temperature bias increases by 1-2 K for most regions compared to AN and SN, consistent with the degradation in the 500-hPa fields (Fig. 11). The biases of 5th and 95th percentile daily averaged 2-m temperature for all sensitivity simulations indicates that the temperature bias is larger in the winter than in the summer. Overall, the sensitivity simulations show that reducing the strength of interior nudging above the PBL domain does not strongly degrade the 2-m temperature. These results also support the use of non-zero nudging coefficients on the inner nest regardless of the interior nudging technique. Without the interior constraint from either analysis or spectral nudging on the inner nest, the large-scale flow over the Rocky Mountains is less consistent with the driving fields, which contributes to increased errors in mean 2-m temperature bias for the Plains and Midwest regions.

Unlike for 500-hPa geopotential height and 2-m temperature, the changes in precipitation bias do not increase toward the center of the 36-km domain when the interior nudging strengths are reduced (Table 3). For most of the regions, the mean precipitation bias generally increases across the 36-km domain as the nudging strengths are decreased in (ANlow and SNlow) and removed from (ANouter and SNouter) that domain. Both analysis and spectral nudging have qualitatively similar responses to the changes in nudging strength on the 36-km domain. The mean precipiation bias is largest in the Northeast. The 95th percentile of precipitation reveals that the intensity of precipitation events generally increases as the nudging strength on the inner domain is reduced. These results demonstrate that the choice of nudging strategy may affect the statistics of extreme events, with important implications for regional climate modeling applications. On the other hand, the Southwest region has similar biases regardless of the nudging technique, which demonstrates that nudging may mitigate but cannot always overcome deficiencies in the physics of the RCM.

In Fig. 13, the spectra of 250-hPa zonal wind are used to gauge changes in variability due to interior nudging as the nudging strength on the 36-km domain is progressively reduced. When the nudging coefficients are reduced by one order of magnitude on both domains (ANlow and SNlow) compared to AN and SN, the SNlow variability is qualitatively similar to SN (refer to Fig. 10) for both January and July. In SN and SNlow, the variability approaches but is consistently lower than that in NN (where no interior nudging was used on either domain) for all wavelengths. Thus, reducing the nudging coefficient on the 36-km domain by one order of magnitude has little impact on the variability of the 250-hPa zonal wind generated by the spectral nudging technique. By contrast, reducing the nudging coefficient for analysis nudging (comparing ANlow in Fig. 13 to AN in Fig. 10) shows that there is a marked increase in variability by lowering the nudging coefficient. When non-zero nudging coefficients are used for analysis nudging on the 36-km domain, the analysis nudging simulations have consistently lower variability than NN, SN, and SNlow, but the variability in the ANlow case is more similar to NARR than AN is. Nudging only on the outer (108-km) domain (ANouter and SNouter in Fig. 13) results in more variability for the nested (36-km) domain in both January and July, particularly for SNouter. During July, ANouter and SNouter both generate consistently greater variability than NN at all wavelengths. Despite adding variability at the length scales resolvable in the RCM but not in the coarse input reanalysis, there are still large errors in the large-scale circulation and near-surface features that adversely affect the quality of the RCM simulation when interior nudging is not used on the 36-km domain (Figs. 11 and 12). Balancing the consistency of the RCM simulation with the input data set (by using interior nudging techniques more strongly) against the freedom of the RCM to generate variability at finer scales than the input data (by nudging more weakly) remains a challenge for downscaling.

4. Conclusions and future research

This study compared the three nudging techniques in the WRF model using two-way nesting to determine the influence of interior nudging on mean error and added variability over an annual cycle for regional climate modeling applications. The WRF model was used to downscale the 2.5º x 2.5º R-2 using a 108- and 36-km two-way nested configuration over the CONUS. WRF was run using nudging only at the lateral boundaries (i.e., no interior nudging), using interior nudging toward differences between WRF and R-2 at individual grid points (i.e., analysis nudging), and using interior nudging toward differences in large-scale waves between WRF and R-2 (i.e., spectral nudging). Sensitivity simulations were conducted where the strength of the nudging was broadly reduced either for both domains or for the 36-km domain only. In each simulation, the interior nudging was restricted to the layers above the PBL. Evaluation of mean regional biases using the 32-km NARR data for daily, monthly, seasonal, and annual scales was performed along with the bias for the 5th and 95th percentile for temperature and 95th percentile for precipitation.

Without interior nudging, the WRF 36-km simulation was wetter and warmer than was observed in each season. Additionally, large positive biases in the seasonally averaged 500-hPa geopotential height occurred when no interior nudging was used, which indicates errors in the large-scale circulation. Both the analysis nudging and spectral nudging techniques were effective at reducing the mean biases in the 500-hPa geopotential height, 850-hPa meridional wind, and 2-m temperature. The precipitation intensity and frequency generated using the analysis nudging technique was overall closer to observations than using spectral nudging or no interior nudging. Additionally, the precipitation amounts and annual cycle were better represented with analysis nudging. The moisture field is not directly adjusted when using spectral nudging in WRF. The better simulation of precipitation achieved by AN than SN suggests that directly nudging moisture may be needed to improve the simulation of precipitation.

The spectra calculation of 250-hPa zonal winds for the WRF simulations, the R-2, and NARR fields showed that the variability was greater with spectral nudging than analysis nudging. Even with reduced (and non-zero) nudging coefficients, analysis nudging dampened the spectral energy compared to both spectral nudging and no interior nudging. Reducing the nudging coefficients for analysis nudging increased the variability compared to the stronger coefficients for analysis nudging and was found to be closer to NARR. When spectral nudging or analysis nudging was applied to the 108-km domain only and there was no interior nudging on the 36-km domain, the variability in the zonal winds aloft increased at all wavelengths compared with not using interior nudging on either domain; however, restricting the nudging to the 108-km domain worsened the representation of the large-scale circulation and 2-m temperature in the 36-km domain. How each nudging technique is applied can greatly impact the results. Our results indicate that interior nudging can reduce mean errors, and nudging more strongly reduces error at the expense of also reducing variability.

Our study demonstrates that both types of interior nudging can be used effectively in WRF in a two-way-interactive nested model to broadly capture large-scale features from the driving model for regional climate modeling. Analysis nudging and spectral nudging each achieve a reduction of bias in 2-m temperature, precipitation, 850-hPa meridional wind, and 500-hPa geopotential height compared to restricting the influence of the input fields only to the lateral boundaries. In addition, we showed that interior nudging should be used on both domains of a two-way nest (and not limited to the outer domain) to improve the near-surface and large-scale fields on the inner domain. As in Lo et al. (2008), we found that analysis nudging was preferable to not using interior nudging at all to achieve consistency with the input fields and to increase accuracy. For some aspects of the evaluation, analysis nudging outperformed spectral nudging, and vice versa, so a case could be made to use either interior nudging technique. However, neither interior nudging technique yielded perfect results or completely overcame the physical and dynamical deficiences and inconsistencies in WRF. We suggest that the default settings for both analysis nudging and spectral nudging in WRF be revisited for regional climate modeling applications, and further work is needed to optimize those settings. Continuous, multi-year integrations driven by reanalysis data are required to verify extreme climatic events and show not only added variability but also added value. Multi-year integrations are also necessary to diagnose the influence of interior nudging on interannual variability. Our results also suggest that the strengths of the nudging coefficients should be minimized for analysis nudging to increase the variability at wavelengths that should be resolvable in the RCM. Further studies are needed to optimize the nudging strategy to simultaneously increase the variability, improve the representation of the large-scale circulation, and reduce errors near the surface. Sensitivity studies are also warranted to understand the influence of nudging throughout the atmospheric column, particularly near the PBL, where nudging too strongly toward coarse input fields could dampen the RCM's ability to generate important mesoscale features near the surface.

Acknowledgments. The authors thank Brian Eder (U.S. EPA) and two anonymous reviewers for their technical reviews of this manuscript. The United States Environmental Protection Agency through its Office of Research and Development funded and managed the research described here. It has been subjected to the Agency's administrative review and approved for publication.

References

Alexandru, A., R. de Elia, R. Laprise, L. Separovic, and S. Biner, 2009: Sensitivity Study of Regional Climate Model Simulations to Large-Scale Nudging Parameters. *Mon. Weather Rev.*, **137**, 1666–1686, doi:10.1175/2008MWR2620.1.

Bukovsky, M. S. and D. J. Karoly, 2007: A Brief Evaluation of Precipitation from the North American Regional Reanalysis. *J. Hydrometeor*, **8**, 837–846, doi:10.1175/JHM595.1.

— 2009: Precipitation Simulations Using WRF as a Nested Regional Climate Model. *J. Appl. Meteor. Climatol.*, **48**, 2152–2159, doi:10.1175/2009JAMC2186.1.

Castro, C. L., R. A. Pielke, and G. Leoncini, 2005: Dynamical downscaling: Assessment of value retained and added using the Regional Atmospheric Modeling System (RAMS). *J. Geophys. Res.*, **110**, D05108+, doi:10.1029/2004JD004721.

Chen, F. and J. Dudhia, 2001: Coupling an Advanced Land Surface Hydrology Model with the Penn State NCAR MM5 Modeling System. Part I: Model Implementation and Sensitivity. *Mon. Weather Rev.*, **129**, doi:10.1175/1520-0493(2001)129⟨0569:CAALSH⟩2.0.CO;2.

Davies, H. C., 1976: A lateral boundary formulation for multi-level prediction models. *Q. J. Roy. Meteorol. Soc.*, **102**, 405–418, doi:10.1256/smsqj.43209.

de Elía, R., D. Caya, H. Côté, A. Frigon, S. Biner, M. Giguère, D. Paquin, R. Harvey, and D. Plummer, 2008: Evaluation of uncertainties in the CRCM-simulated North American climate. *Climate Dynam.*, **30**, 113–132, doi:10.1007/s00382-007-0288-z.

Denis, B., R. Laprise, D. Caya, and J. Côté, 2002: Downscaling ability of one-way nested regional climate models: the Big-Brother Experiment. *Climate Dynam.*, **18**, 627–646, doi:10.1007/s00382-001-0201-0.

Giorgi, F., 2006: Regional climate modeling: Status and perspectives. *Journal de Physique IV*, **139**, 101–118, doi:10.1051/jp4:2006139008.

Kanamitsu, M., W. Ebisuzaki, J. Woollen, S. Yang, J. J. Hnilo, M. Fiorino, and G. L. Potter, 2002: NCEP-DOE AMIP-II Reanalysis (R-2). *Bull. Am. Meteorol. Soc.*, **83**, 1631–1643, doi:10.1175/BAMS-83-11-1631(2002)083<1631:NAR>;2.3.CO;2.

Kucharski, F., I. Kang, D. Straus, and M. P. King, 2010: Teleconnections in the Atmosphere and Oceans. *Bull. Am. Meteorol. Soc.*, **91**, 381–383, doi:10.1175/2009BAMS2834.1.

Laprise, R., R. de Elía, D. Caya, S. Biner, P. Lucas-Picher, E. Diaconescu, M. Leduc, A. Alexandru, L. Separovic, and Canadian Network for Regional Climate Modelling and Diagnostics, 2008: Challenging some tenets of Regional Climate Modelling. *Meteorol. Atmos. Phys.*, **100**, 3–22, doi:10.1007/s00703-008-0292-9.

Leung, L. R. and W. I. Gustafson, 2005: Potential regional climate change and implications to U.S. air quality. *Geophys. Res. Lett.*, **32**, L16711+.

Leung, L. R., Y.-H. Kuo, and J. Tribbia, 2006: Research Needs and Directions of Regional Climate Modeling Using WRF and CCSM. *Bull. Am. Meteorol. Soc.*, **87**, doi:10.1175/BAMS-87-12-1747.

Leung, R. L. and Y. Qian, 2009: Atmospheric rivers induced heavy precipitation and flooding in the western U.S. simulated by the WRF regional climate model. *Geophys. Res. Lett.*, **36**, L03820+, doi:10.1029/2008GLO36445.

Lo, J. C., Z. Yang, and R. A. Pielke, 2008: Assessment of three dynamical climate downscaling methods using the Weather Research and Forecasting (WRF) model. *J. Geophys. Res.*, **113**, D09112+, doi:10.1029/2007JD009216.

Mesinger, F., G. DiMego, E. Kalnay, K. Mitchell, P. Shafran, W. Ebisuzaki, D. Jović, J. Woollen, E. Rogers, E. H. Berbery, M. B. Ek, Y. Fan, R. Grumbine, W. Higgins, H. Li, Y. Lin, G. Manikin, D. Parrish, and W. Shi, 2006: North American Regional Reanalysis. *Bull. Am. Meteorol. Soc.*, **87**, 343–360, doi:10.1175/BAMS-87-3-343.

Miguez-Macho, G., G. L. Stenchikov, and A. Robock, 2004: Spectral nudging to eliminate the effects of domain position and geometry in regional climate model simulations. *J. Geophys. Res.*, **109**, D13104+, doi:10.1029/2003JD004495.

— 2005: Regional Climate Simulations over North America: Interaction of Local Processes with Improved Large-Scale Flow. *J. Climate*, **18**, 1227–1246, doi:10.1175/JCLI3369.1.

Namias, J., 1991: Spring and Summer 1988 Drought over the Contiguous United States:Causes and Prediction. *J. Climate*, **4**, 54–65, doi:10.1175/1520-0442(1991)004<0054:SASDOT>2.0.CO;2.

Nolte, C. G., A. Gilliland, C. Hogrefe, and L. J. Mickley, 2008: Linking global to regional models to assess future climate impacts on surface ozone levels in the United States. *J. Geophys. Res.*, **113**, D14307+, doi:10.1029/2007JD008497.

Otte, T. L., 2008: The Impact of Nudging in the Meteorological Model for Retrospective Air Quality Simulations. Part I: Evaluation against National Observation Networks. *J. Appl. Meteorol. Clim.*, **47**, 1853–1867, doi:10.1175/2007JAMC1790.1.

Pielke, R. A., 2002: *Mesoscale Meteorological Modeling*. Academic Press, San Diego, CA, 2 edition, 1–676 pp.

Pleim, J. E., J. O. Young, D. Wong, R. C. Gilliam, T. L. Otte, and R. Mathur, 2008: *Two-way coupled meteorology and air quality modeling*, Springer, New York, NY, chapter 2. 235–242.

Rockel, B., C. L. Castro, R. A. Pielke, H. von Storch, and G. Leoncini, 2008: Dynamical downscaling: Assessment of model system dependent retained and added variability for two different regional climate models. *J. Geophys. Res.*, **113**, D21107+, doi:10.1029/2007JD009461.

Salathé, E. P., R. Steed, C. F. Mass, and P. H. Zahn, 2008: A High-Resolution Climate Model for the U.S. Pacific Northwest: Mesoscale Feedbacks and Local Responses to Climate Change. *J. Climate*, **21**, 5708–5726, doi:10.1175/2008JCLI2090.1.

Skamarock, W. C., 2004: Evaluating Mesoscale NWP Models Using Kinetic Energy Spectra. *Mon. Wea. Rev.*, **132**, 3019–3032, doi:10.1175/MWR2830.1.

Skamarock, W. C., J. B. Klemp, J. Dudhia, D. O. Gill, M. Barker, K. G. Duda, X. Y. Huang, W. Wang, and J. G. Powers, 2008: A description of the Advanced Research WRF Version 3. Technical report, National Center for Atmospheric Research.

Stauffer, D. R. and N. L. Seaman, 1994: Multiscale Four-Dimensional Data Assimilation. *J. Appl. Meteorol.*, **33**, 416–434, doi:10.1175/1520-0450(1994)033<0416:MFDDA>2.0.CO;2.

Trenberth, K. E. and C. J. Guillemot, 1996: Physical Processes Involved in the 1988 Drought and 1993 Floods in North America. *J. Climate*, **9**, 1288–1298, doi:10.1175/1520-0442(1996)009<1288:PPIITD>2.0.CO;2.

von Storch, H., H. Langenberg, and F. Feser, 2000: A Spectral Nudging Technique for Dynamical Downscaling Purposes. *Mon. Weather Rev.*, **128**, 3664–3673, doi:10.1175/1520-0493(2000)128<3664:ASNTFD>2.0.CO;2.

Yin, J. H., 2005: A consistent poleward shift of the storm tracks in simulations of 21st century climate. *Geophys. Res. Lett.*, **32**, L18701+, doi:10.1029/2005GL023684.

List of Tables

List of Figures

mm day^{-1}, 101-200 mm day^{-1} and greater than 200 mm day^{-1} at the right tail of the distribution.

Figure 10: Spectra computed for R-2 (dashed black), NARR (solid black), and WRF (NN-blue, AN-red, SN-green) simulations averaged for (a) January and (b) July . Vertical lines indicate 4Δx bounds of wave numbers between which added value can be expected by using a RCM.

Figure 11: 500-hPa geopotential height bias (m) compared to NARR for the fall (OND) season for (a) ANlow, (b) SNlow, (c) ANouter, and (d) SNouter.

Figure 12: 850-hPa meridional wind (m s^{-1}) bias for summer (JJA) in (a) ANlow (b) SNlow (c) ANouter and (d) SNouter.

Figure 13: Spectra computed for R-2 (dashed black), NARR (solid black), and WRF for (a) January ANlow (red) and SNlow (green), (b) July ANlow (red) and SNlow (green), (c) January ANouter (red) and SNouter (green), and (d) July ANouter (red) and SNouter (green).The WRF NN simulation (blue) is plotted for relative comparison. Vertical lines indicate 4Δx bounds of wavenumbers between which added value can be expected by using an RCM.

Table 1: WRF simulations and corresponding nudging coefficients (s^{-1}) for nudging above the PBL. The same nudging strength is applied to both inner and outer domains, except in ANouter and SNouter where nudging is applied to the outer domain only. Here, U and V refer to the grid-relative wind components, T is the potential temperature, Q is the water vapor mixing ratio, and Φ is the geopotential.

	Nudging Coefficient (s^{-1})			
Simulation	U / V	T	Q	Φ
NN	-	-	-	-
AN	$3*10^{-4}$	$3*10^{-4}$	$1*10^{-4}$	-
ANlow	$3*10^{-5}$	$3*10^{-5}$	$1*10^{-5}$	-
ANouter	$3*10^{-4}$	$3*10^{-4}$	$1*10^{-4}$	-
SN	$3*10^{-4}$	$3*10^{-4}$	-	$3*10^{-4}$
SNlow	$3*10^{-5}$	$3*10^{-5}$	-	$3*10^{-5}$
SNouter	$3*10^{-4}$	$3*10^{-4}$	-	$3*10^{-4}$

Table 2: Bias of the 5^{th} percentile, mean, and 95^{th}percentile daily averaged 2-m temperature (K) over 1988 for each of the regions shown in Fig. 1..

	Temperature Bias 5th Percentile / Mean / 95th Percentile					
	NW	SW	PL	MW	SE	NE
NN	2.8 / 1.8 / 2.1	2.9 / 2.3 / 1.8	6.2 / 4.3 / 3.7	3.9 / 2.5 / -0.8	4.1 / 2.5 / 1.8	1.8 / 1.2 / -1.9
AN	-0.4 / -0.2 / -0.7	0.1 /-0.1 / -0.7	4.2 / 2.4 / 1.0	3.4 / 1.8 / 0.2	2.0 / 1.0 / -0.4	0.9 / 0.8 / -0.9
ANlow	0.4 / 0.1 / -0.7	1.0 / 0.3 / -0.1	4.1 / 2.4 / 1.3	2.8 / 1.6 / 0.4	1.8 / 1.0 / -0.3	1.2 / 0.8 / -0.6
ANouter	1.4 / 0.8 / 0.2	2.3 / 1.9 / 1.4	4.2 / 3.2 / 2.0	2.1 / 1.6 / -0.6	2.3 / 2.0 / 2.2	0.9 / 0.7 / -1.2
SN	-0.7 / -0.5 / -0.8	-0.3 / -0.3 / -0.6	2.9 / 1.6 / 0.2	2.5 / 0.9 / -0.9	1.8 / 0.6 / -0.7	0.1 / 0.4 / -1.0
SNlow	0.1 / -0.1 / -0.8	1.0 / 0.2 / -0.3	3.7 / 2.0 / 1.1	2.4 / 1.1 / -0.4	1.8 / 0.9 / 0.0	0.9 / 0.5 / -1.0
SNouter	0.8 / 0.5 / 0.2	1.8 / 1.7 / 1.4	4.0 / 3.5 / 3.4	3.2 / 1.9 / 1.2	2.6 / 2.2 / 2.8	0.9 / 0.6 / -0.4

Table 3: Bias of the mean and 95th percentile daily averaged precipitation (mm day^{-1}) over 1988 for each of the regions shown in Fig. 1.

	Precipitation Bias Mean / 95th Percentile					
	NW	SW	PL	MW	SE	NE
NN	0.9 / 2.5	0.5 / 0.9	0.3 / 0.0	0.7 / 2.5	1.3 / 3.0	1.6 / 6.1
AN	0.0 / 0.4	0.1 / 0.3	0.0 / -0.2	-0.6 / -1.2	0.5 / 0.9	1.1 / 2.5
ANlow	0.6 / 2.3	0.4 / 1.1	0.5 / 1.5	0.3 / 1.3	1.0 / 1.9	1.0 / 3.2
ANouter	1.0 / 3.3	0.5 / 1.4	0.5 / 0.3	0.9 / 2.3	1.3 / 3.1	2.3 / 6.8
SN	0.8 / 1.2	0.4 / 0.8	0.6 / 0.7	0.5 / 2.6	0.7 / 0.5	1.1 / 2.5
SNlow	0.9 / 2.1	0.5 / 1.2	0.6 / 1.6	0.6 / 3.0	0.8 / 1.6	1.6 / 3.6
SNouter	1.0 / 2.1	0.6 / 1.4	-0.1 / -1.0	0.6 / 1.8	0.8 / 2.5	2.5 / 8.4

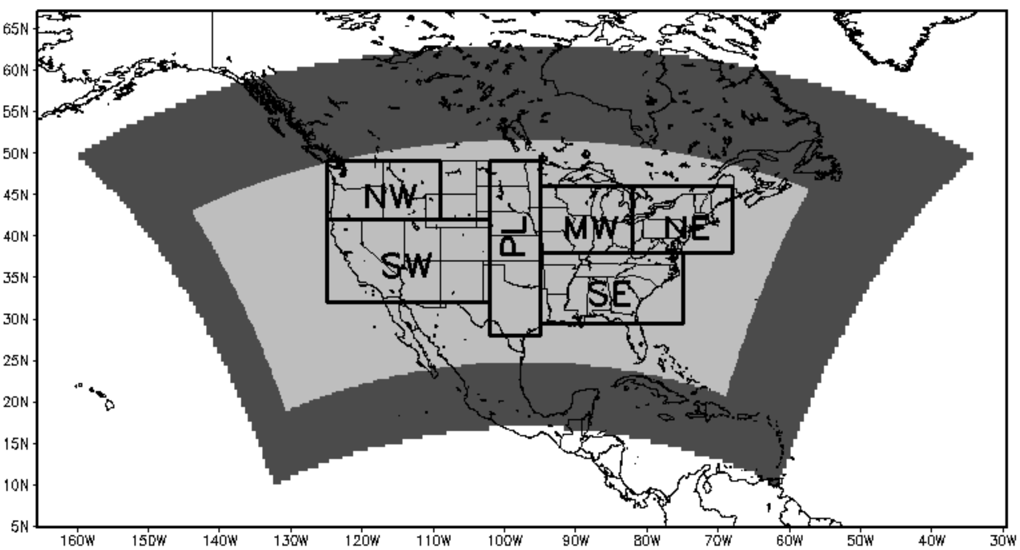

Figure 1: WRF outer (108-km) and inner (36-km) domains. Box regions used for model evaluation: Northwest (NW), Southwest (SW), Plains (PL), Midwest (MW), Southeast (SE), and Northeast (NE).

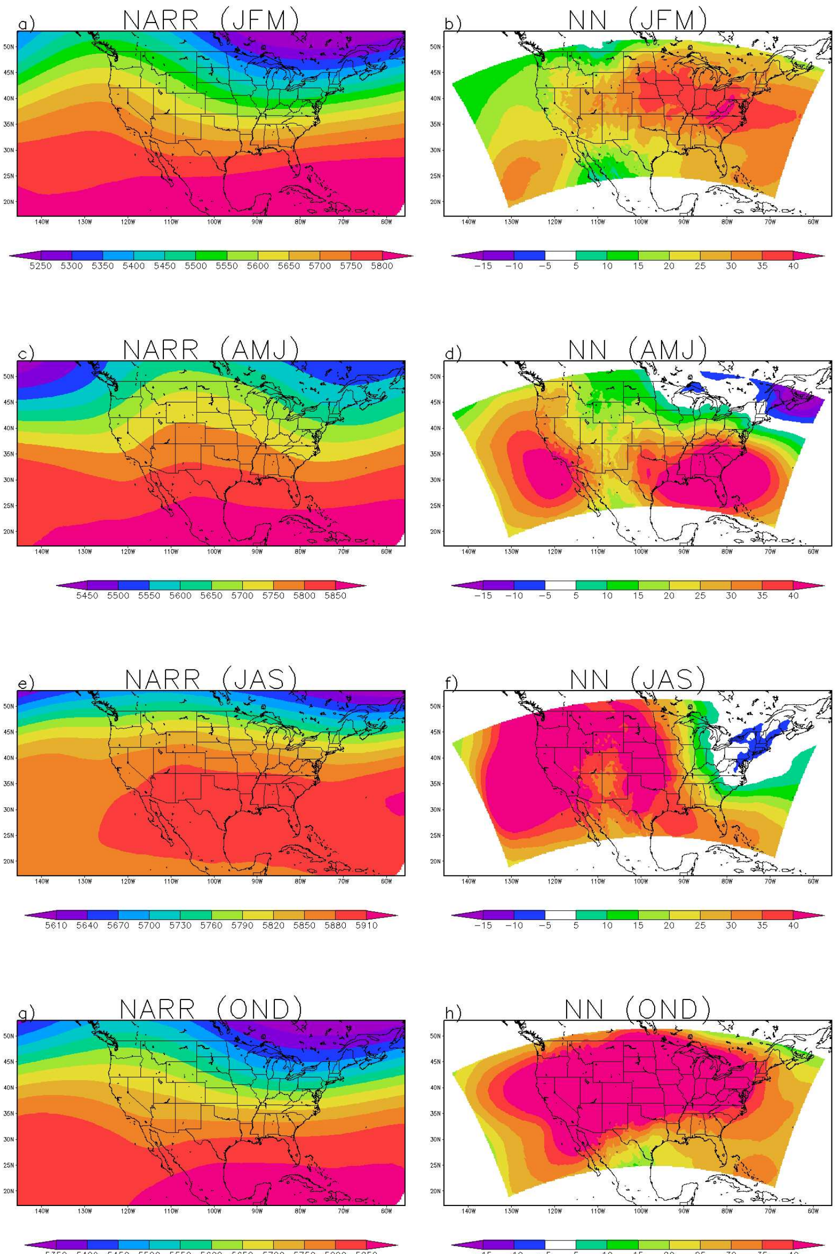

Figure 2: 500-hPa seasonal geopotential height (m) for NARR (a) JFM, (c) AMJ, (e) JAS, (g) OND and model seasonal bias of 500-hPa geopotenial height (m) for the NN configuration (b) JFM, (d) AMJ, (f) JAS, (h) OND.

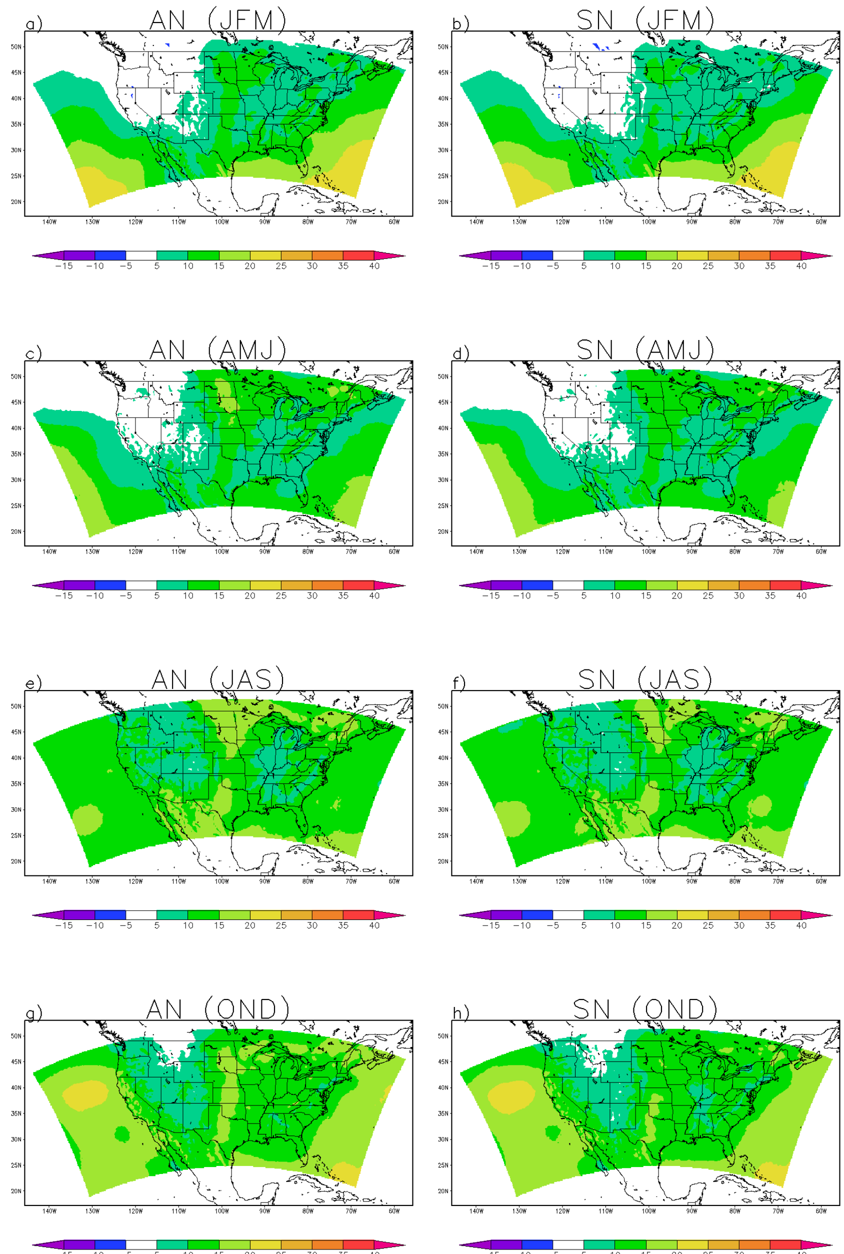

Figure 3: 500-hPa geopotential height bias (m) for AN (a) JFM, (c) AMJ, (e) JAS, (g) OND and SN (b) JFM, (d) AMJ, (f) JAS, (h) OND.

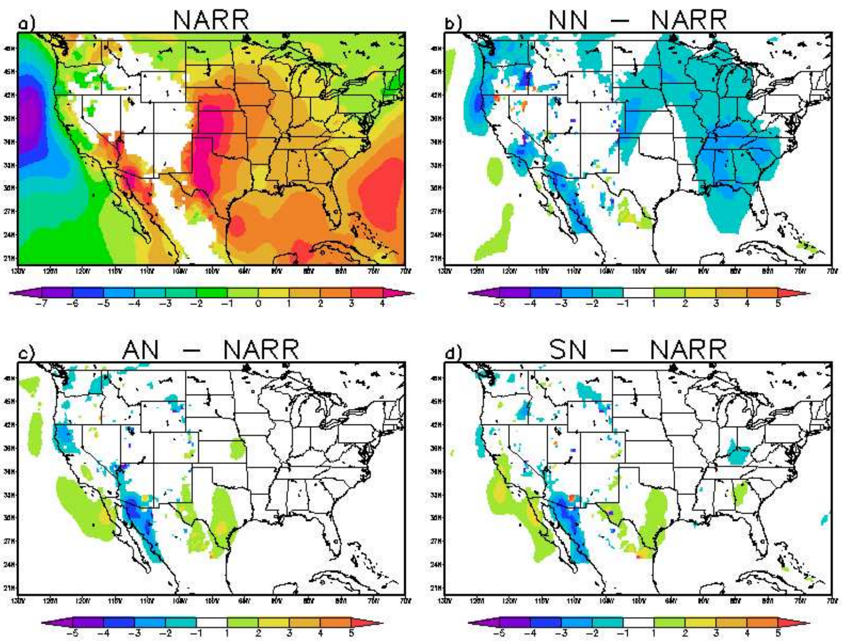

Figure 4: 850-hPa meridional wind (m s^{-1}) for summer (JJA) in (a) NARR and meridional wind bias for (b) NN, (c) AN, and (d) SN.

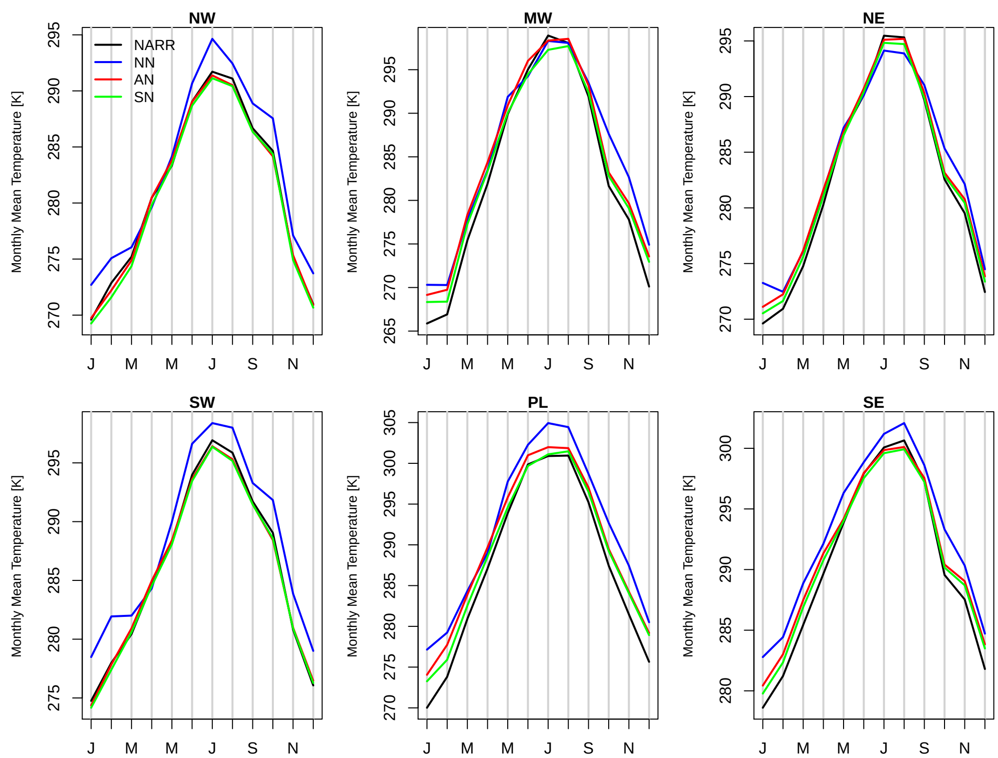

Figure 5: Mean monthly 2-m temperature (K) for each of the six verification regions shown in Fig. 1 for NARR (black), NN (blue), AN (red), and SN (green).

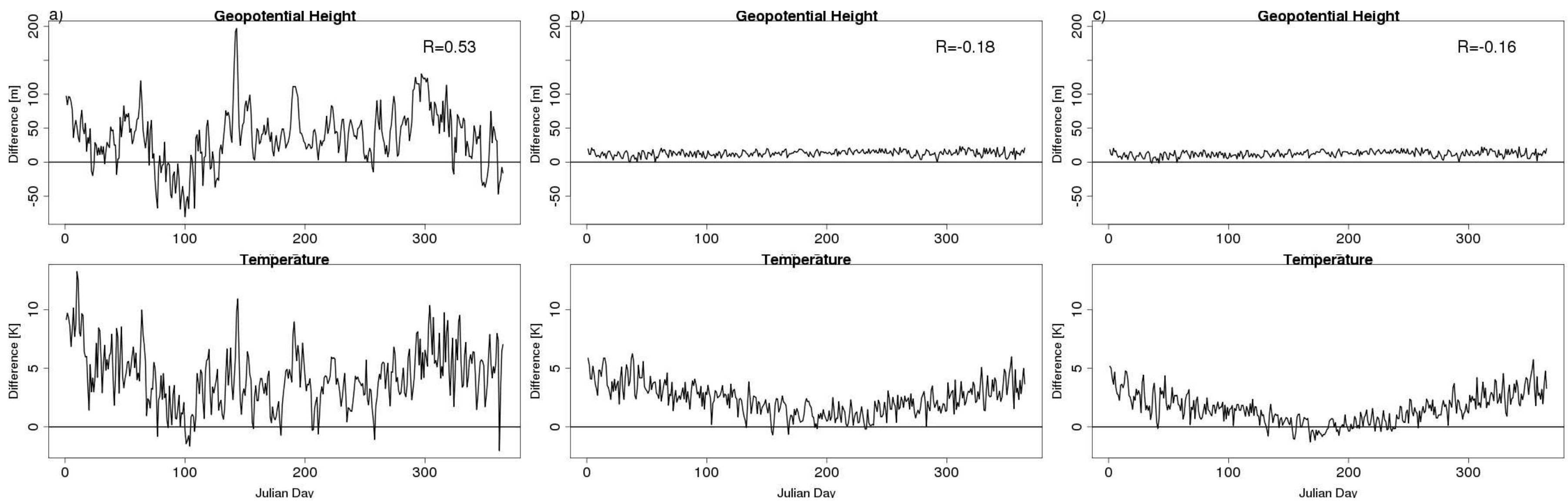

Figure 6: Daily averaged 500-hPa geopotential height bias (top) and 2-m temperature bias (bottom) for the Plains region for (a) NN (b) AN (c) SN. The correlation coefficient between the daily geopotential height bias and temperature bias is shown.

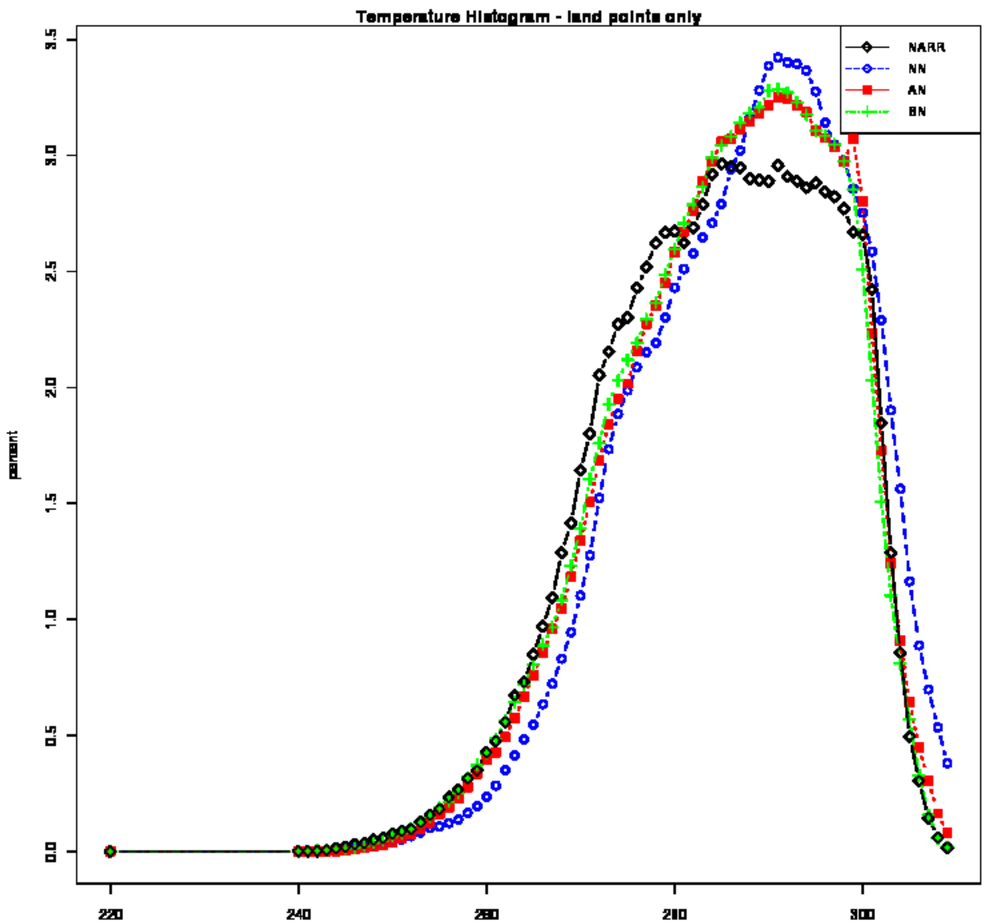

Figure 7: Daily 2-m temperature distribution for land points in the 36-km domain for 1988 comparing NN (blue), AN (red), and SN (green) to NARR (black). The first bin is 220-240 K; subsequent bins are at 1 K intervals to 310 K.

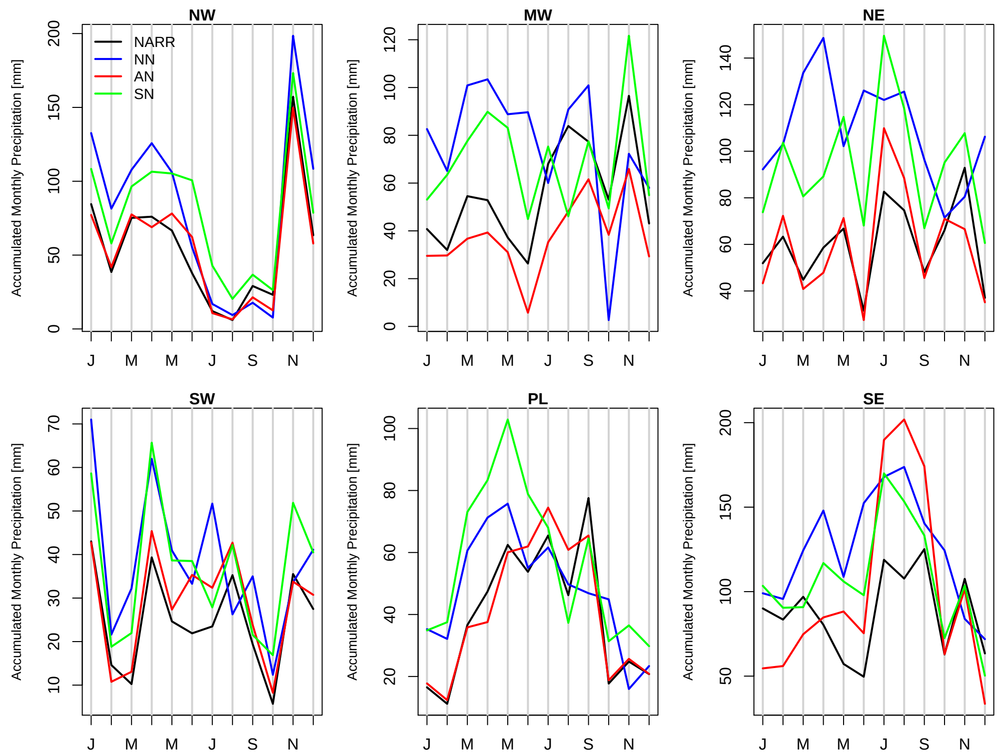

Figure 8: Accumulated monthly precipitation (mm) for each of the six verification regions shown in Fig.1 NARR (black), NN (blue), AN (red), and SN (green).

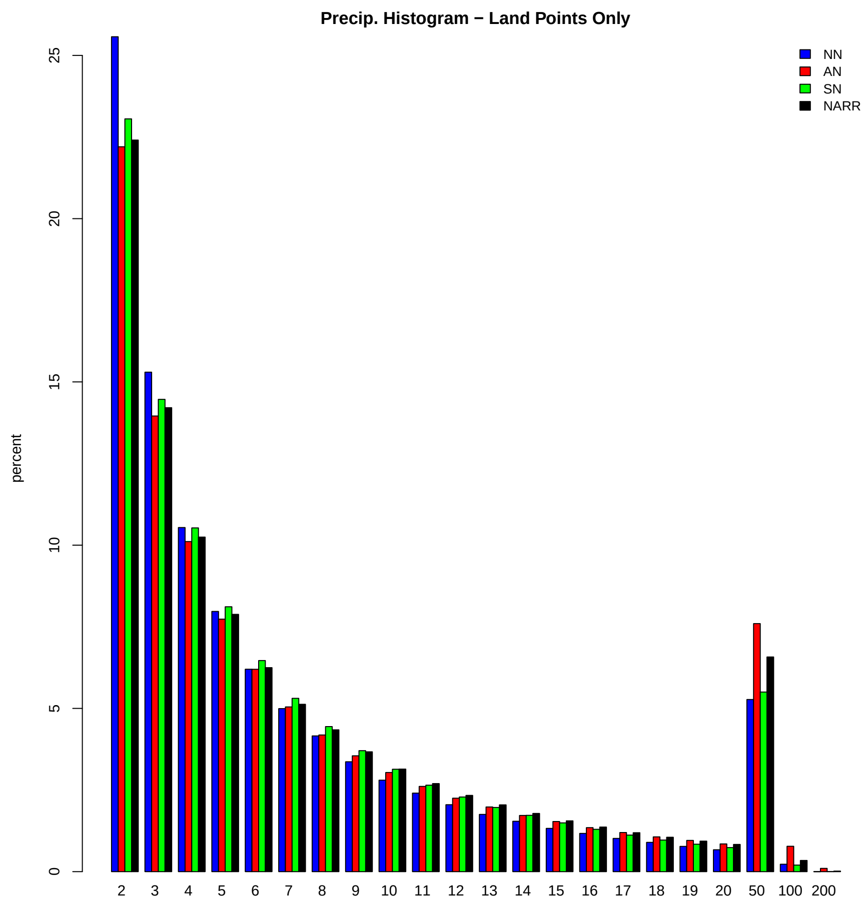

Figure 9: Daily precipitation distribution for land points in the 36-km domain from the annual WRF simulations comparing the NN (blue), AN (red), and SN (green) to NARR observations (black). The x-axis represents the precipitation bins (mm day^{-1}) omitting the 0-1 mm day^{-1} bin with 1 mm day^{-1} bins up to 20 mm day^{-1} with larger bins of 21-50 mm day^{-1}, 51-100 mm day^{-1}, 101-200 mm day^{-1} and greater than 200 mm day^{-1} at the right tail of the distribution.

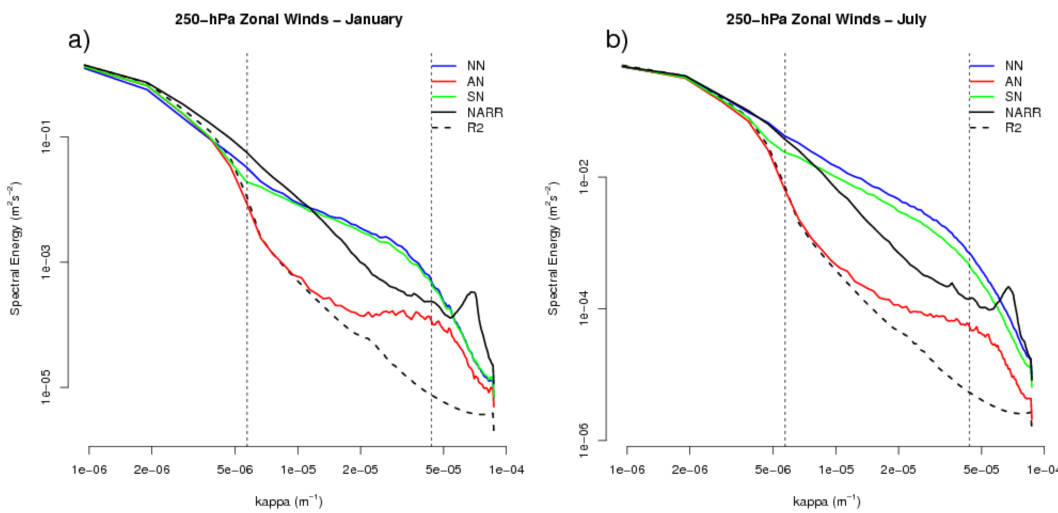

Figure 10: Spectra computed for R-2 (dashed black), NARR (solid black), and WRF (NN-blue, AN-red, SN-green) simulations averaged for (a) January and (b) July . Vertical lines indicate 4Δx bounds of wave numbers between which added value can be expected by using a RCM.

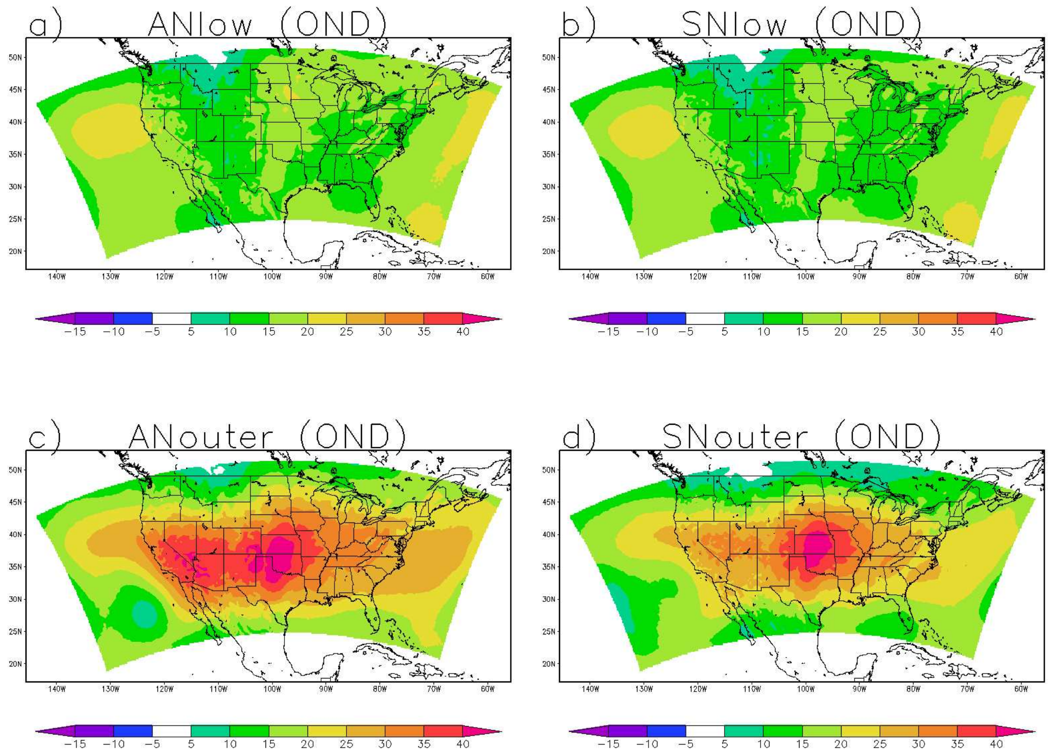

Figure 11: 500-hPa geopotential height bias (m) compared to NARR for the fall (OND) season for (a) ANlow, (b) SNlow, (c) ANouter, and (d) SNouter.

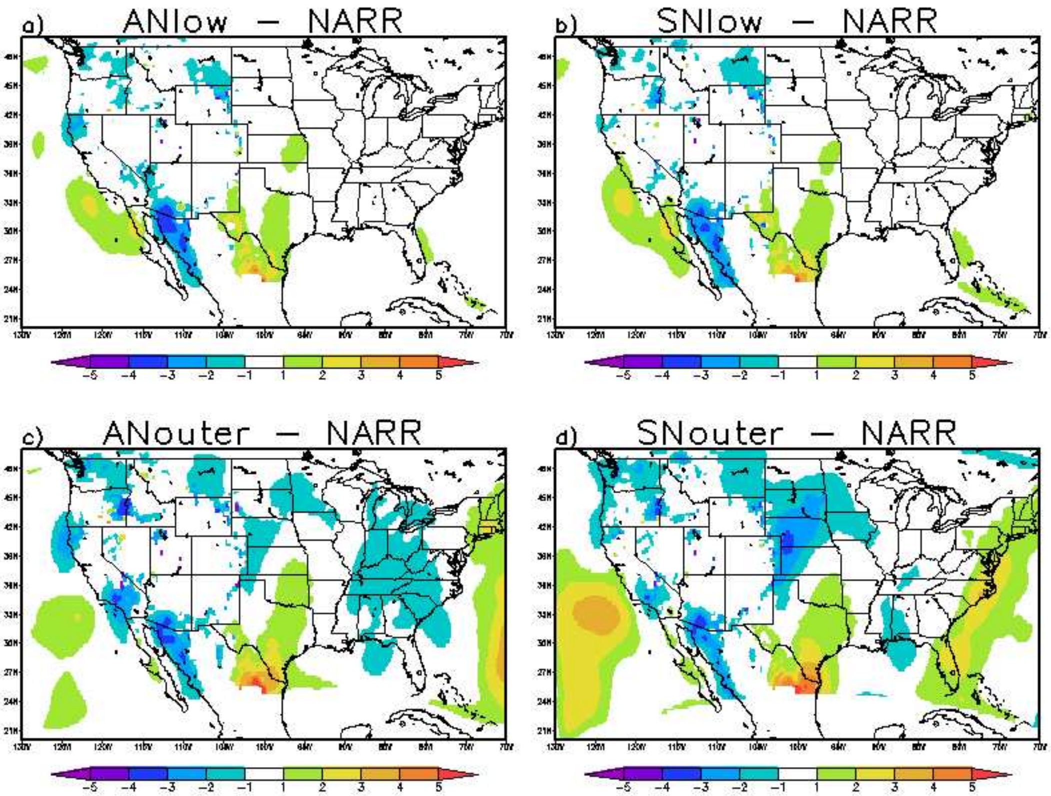

Figure 12: 850-hPa meridional wind (m s^{-1}) bias for summer (JJA) in (a) ANlow (b) SNlow (c) ANouter and (d) SNouter.

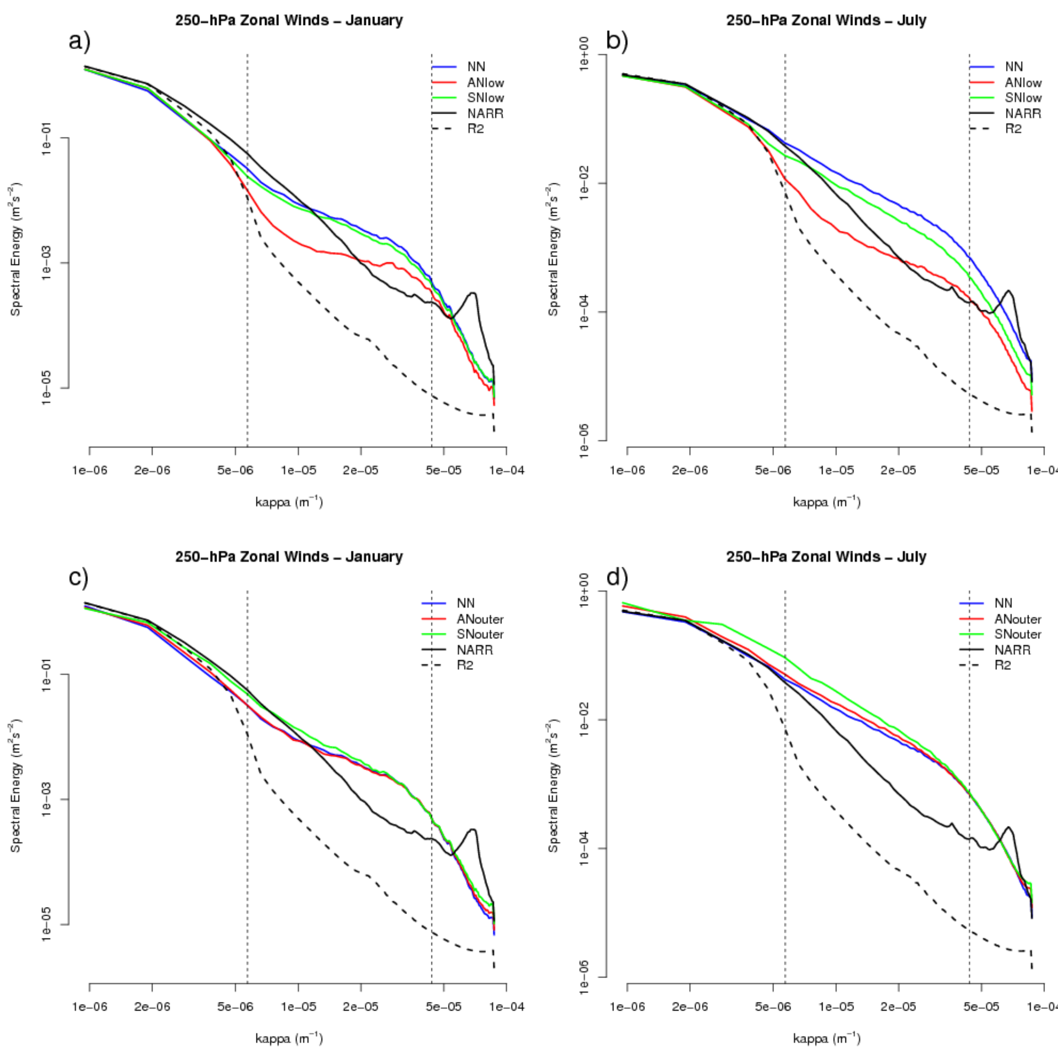

Figure 13: Spectra computed for R-2 (dashed black), NARR (solid black), and WRF for (a) January ANlow (red) and SNlow (green), (b) July ANlow (red) and SNlow (green), (c) January ANouter (red) and SNouter (green), and (d) July ANouter (red) and SNouter (green). The WRF NN simulation (blue) is plotted for relative comparison. Vertical lines indicate $4\Delta x$ bounds of wavenumbers between which added value can be expected by using an RCM.